

Quantum simulations of Fermionic Hamiltonians with efficient encoding and ansatz schemes

Benchen Huang,[†] Nan Sheng,[†] Marco Govoni,^{*,‡,¶} and Giulia Galli^{*,‡,§,¶}

[†]*Department of Chemistry, University of Chicago, Chicago, IL 60637, USA*

[‡]*Pritzker School of Molecular Engineering, University of Chicago, Chicago, IL 60637, USA.*

[¶]*Materials Science Division and Center for Molecular Engineering, Argonne National Laboratory, Lemont, IL 60439, USA.*

[§]*Department of Chemistry, University of Chicago, Chicago, IL 60637, USA.*

E-mail: mgovoni@anl.gov; gagalli@uchicago.edu

Abstract

We propose a computational protocol for quantum simulations of Fermionic Hamiltonians on a quantum computer, enabling calculations on spin defect systems which were previously not feasible using conventional encodings and unitary coupled-cluster ansatz of variational quantum eigensolvers. We combine a qubit-efficient encoding scheme mapping Slater determinants onto qubits with a modified qubit-coupled cluster ansatz and noise-mitigation techniques. Our strategy leads to a substantial improvement in the scaling of circuit gate counts and in the number of required qubits, and to a decrease in the number of required variational parameters, thus increasing the resilience to noise. We present results for spin defects of interest for quantum technologies, going beyond minimum models for the negatively charged nitrogen vacancy center in diamond and the double vacancy in 4H silicon carbide (4H-SiC) and tackling a defect as complex as negatively charged silicon vacancy in 4H-SiC for the first time.

1 Introduction

Obtaining accurate solutions of the electronic structure of many-body systems is a major challenge in computational science, and an important endeavor that may benefit problems in several fields, ranging from catalysis¹⁻³ and drug discovery⁴ to quantum technologies.^{5,6} In addition to steady efforts in the development of algorithms to solve the electronic structure problem on classical computers, research into the use of quantum computers to solve the time independent Schrödinger equation has been flourishing in the past decades.⁷⁻¹⁴ The motivation behind this trend is the promise that a fault-tolerant quantum computer may be able to solve the electronic structure problem for many-body systems¹⁵ in polynomial time, for example using a quantum phase estimation (QPE)^{7,16-18} algorithm. The latter is a probabilistic method to obtain the eigenstate of a unitary operator that assumes that the initial state of a given system, prepared on a quantum computer, has a non vanishing overlap with the target state.

The possibility of reaching exponential quantum advantage for quantum chemistry problems remains controversial.¹⁹ However, it is interesting to explore whether quantum computers may in fact turn out to be advantageous over classical ones, even in the absence of exact polynomial scaling, and in particular whether even today’s noisy intermediate scale quantum (NISQ) platforms may be utilized for interesting problems. Recent efforts^{14,20,21} to incorporate quantum computations into quantum Monte Carlo methods²² suggest new route for such benefits to be achieved, in practice, even with noisy hardware. Specifically, Ref¹⁴ reported a calculation of the atomization energy of the strongly correlated square H₄ molecule, using a quantum-classical hybrid quantum Monte Carlo method on the Sycamore quantum processor,²³ which achieved accuracy that is competitive with state-of-the-art classical methods. The algorithm relies on the preparation of a so called *a priori* quantum trial state on the quantum hardware, which is considered as an approximation to the target ground state. Therefore it appears that one strategy to obtain computational advantage on both NISQ and fault-tolerant quantum devices, relies on the efficient preparation of an ac-

curate initial state; this strategy has been explored for both molecular^{8,24–35} and condensed systems.^{36–40}

An appealing and popular protocol to obtain the ground state of Fermionic systems is that of writing the Hamiltonian in second quantization and using a variational quantum eigensolver (VQE).^{8,41} This algorithm parameterizes the many-body wavefunction through a quantum circuit, and the energy is measured on a noisy hardware. Upon optimization of the parameters on classical hardware, one obtains a variational upper bound on the ground state energy. The efficiency and reliability of VQE depend on the number of available qubits on the quantum hardware, on the qubit coherence time and usually VQE faces optimization challenges due to the hardware noise. However, despite these challenges, this algorithm has been successfully applied to study systems with up to 12 electrons.³⁰

In a recent paper, we utilized VQE to solve the electronic structure of the minimum model of realistic solid state systems with strongly correlated states, and we carried out calculations on a quantum computer. In particular we considered spin-defects in solids, i.e. the negatively charged nitrogen vacancy center (NV^-) in diamond and the neutral di-vacancy (VV^0) in 4H-SiC,⁴⁰ which are of interest for quantum information applications,^{42,43} including quantum sensing,⁴⁴ communication⁴⁵ and bioimaging.⁴⁶ Although we obtained encouraging results, we also identified several problems awaiting for more efficient and accurate solutions. For example, the so called unphysical state problem,⁴⁷ caused by an imperfect conservation of the number of particles on a noisy hardware, leads to values of the energy that lie below the exact classical reference value. We solved this problem by post selecting⁴⁸ the measured values of the energy and considering only those corresponding to the correct number of particles. The combination of post-selection and zero-noise extrapolation (ZNE) techniques^{49–52} led us to solve the electronic structure of realistic spin-defects. However, we could do so only for minimum models, as the ansatz circuit used in VQE usually leads to a large gate count and hence calculations are hard to scale.

Here we propose a computational strategy leading to an improved scaling with gate counts

of VQE optimizations, thus enabling electronic structure calculations of complex spin-defects previously not feasible with conventional VQE algorithms. In particular, we combine a qubit-efficient encoding (QEE) scheme⁵³ with a modified qubit-coupled cluster (QCC) ansatz⁵⁴ and noise-mitigation techniques. Such a protocol leads to a substantial decrease in the number of required variational parameters in VQE calculations, thus increasing the resilience to noise and enabling calculations of spin defects beyond the minimum model.⁴⁰ The rest of the paper is organized as follows. In Section 2 we discuss the quantum algorithms adopted to solve the electronic structure of systems whose parametrized Hamiltonian is expressed in second quantization. In Section 3, we present calculations on a real quantum computer of three spin defect systems, i.e. NV^- in diamond, VV^0 and a new defect—negatively charged silicon vacancy (V_{Si}^-) in 4H-SiC, which for some applications^{55,56} is a promising alternative to NV centers. Section 4 concludes our work with a summary and outlook.

2 Methods

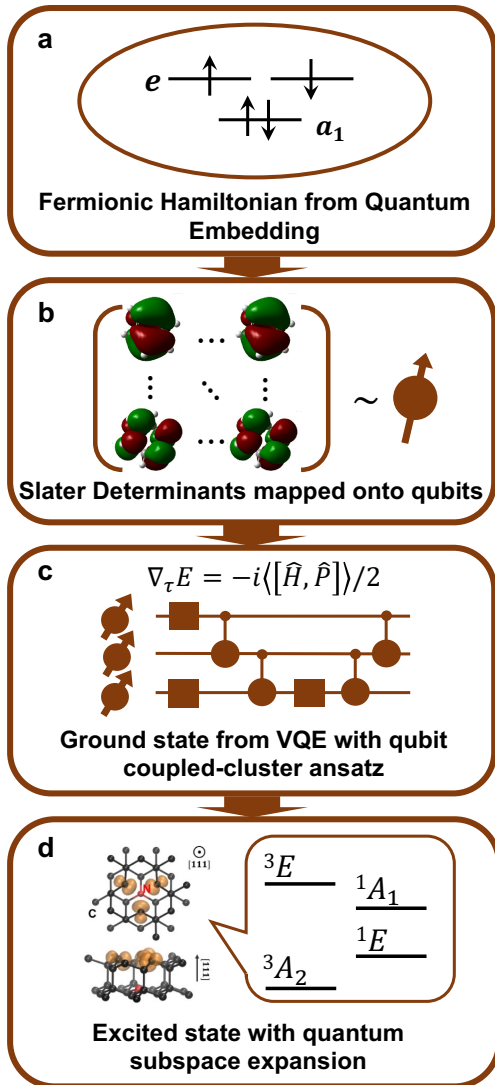


Figure 1: Workflow used to simulate the ground and excited state energies of spin defects on a quantum computer. **a** The effective Hamiltonian in second quantization describing the electronic structure of spin defects is obtained from a quantum defect embedding theory (QDET), see Sec 3.1 for detail. **b** The Slater determinants are mapped onto qubits using a qubit-efficient encoding scheme, where the molecular orbitals represent a Slater Determinant. **c** The ground state of the effective Hamiltonian is obtained using a variational quantum eigensolver (VQE) and a qubit coupled-cluster (QCC) ansatz. **d** The excited states of the effective Hamiltonian are obtained using a quantum subspace expansion (QSE) algorithm.

The workflow adopted here to obtain the ground and excited states of a Fermionic Hamiltonian \hat{H}_{elec} on a quantum computer is summarized in Fig. 1 and consists of the following

steps: (i) define a Fermionic Hamiltonian using a quantum defect embedding theory (QDET), (ii) derive a qubit Hamiltonian by mapping selected electronic configurations (Slater determinants) of the Fermionic Hamiltonian onto qubits, (iii) compute the ground state energy of the qubit Hamiltonian using VQE, (iv) compute the excited states using the quantum subspace expansion (QSE) algorithm. The qubit Hamiltonian $\hat{H}_q = \sum_i g_i \hat{P}_i$ contains coefficients g_i obtained from the one- and two- body terms of \hat{H}_{elec} multiplied by Pauli strings, i.e., $\hat{P}_i \in \{I, X, Y, Z\}^{\otimes N_q}$, where N_q is the number of qubits and I, X, Y, Z are Pauli operators. When using a VQE algorithm, an ansatz circuit, usually a parametrized unitary operator $\hat{U}(\vec{\theta})$, is defined and applied to a chosen initial state $|\Psi_0\rangle$. Finally, the ground state energy E_g is variationally obtained by optimizing the parameters $\vec{\theta}$ of the ansatz such that $E_g = \min_{\vec{\theta}} \langle \Psi_0 | \hat{U}^\dagger(\vec{\theta}) \hat{H} \hat{U}(\vec{\theta}) | \Psi_0 \rangle$. As mentioned above, excited states are obtained with the QSE algorithm.

For a detailed discussion of the derivation of a Fermionic Hamiltonian describing spin defects in solids using QDET we refer the reader to Ref. ^{36,57–59} Below we discuss in details steps (ii–iv: see panels **b–d** of Fig. 1).

2.1 Qubit Efficient Encoding for Fermionic Mapping

The Fermion to qubit encoding is an isometry $\mathcal{E} : \mathcal{H}_{\text{elec}} \rightarrow \mathcal{H}_q$,⁶⁰ where $\mathcal{H}_{\text{elec}}$ and \mathcal{H}_q represent the physical and qubit Hilbert space spanned by the eigenvectors of \hat{H}_{elec} and \hat{H}_q , respectively. Commonly used encoding schemes such as the Jordan–Wigner (JW),⁶¹ Bravyi–Kitaev (BK)⁶² and parity encoding methods⁶⁰ require $N_q = N$ qubits for a system with N spin-orbitals, and generate a 2^N -dimensional \mathcal{H}_q . However, our goal is to compute the eigenvectors and eigenvalues of \hat{H}_{elec} subject to specific physical constraint on the number of electrons in the two spin channels (m_\uparrow, m_\downarrow). In practice this constraint can be enforced by restricting the solutions of the VQE or QSE algorithms to a subspace of the qubit Hilbert space with dimension $Q = \binom{N/2}{m_\uparrow} \times \binom{N/2}{m_\downarrow} < 2^N$. However, the JW and BK encoding maps do not enforce such a physical constraint and thus lead to a qubit Hilbert space that is

larger than the physical one,⁴⁷ e.g., the former contains all Fock states, some corresponding to a number of electrons different from those of the physical system. In principle, on a fault-tolerant computer the VQE algorithm should preserve the initial number of electrons throughout the optimization process; however, the noise present in NISQ devices does not guarantee the preservation of the physical constraints,⁶³ leading to errors in ground state energies that in Ref.⁴⁰ we have mitigated with a post-selection procedure. Note that other symmetry constraints, e.g., point group symmetry⁶⁴ could also be taken into account when choosing relevant Slater determinants, which would be interesting to explore in future works.

Here we adopt instead the QEE scheme,⁵³ a compact Fermion to qubit encoding map^{65–67} that by definition excludes from the qubit Hilbert space all Fock states with nonphysical number of electrons, leading to a robust solution of the unphysical state problem. The QEE encoding has also the benefit of requiring a smaller number of qubits than the conventional encoding maps. The use of QEE has already been shown to be beneficial on quantum hardware⁵³ for molecules such as H₂ and LiH; here we show that its use is crucial in the case of spin-defects, where the number of qubits required to go beyond minimum models by conventional encodings would be impractical on NISQ devices.

In the QEE scheme, one pre-selects all the electronic configurations $\mathcal{F} = \{|\mathbf{f}\rangle_i \mid |\mathbf{f}\rangle_i \in \mathcal{H}_{\text{elec}}\}$ that satisfy the required set of physical constraints, e.g., fixed number of particles and fixed spin projection \hat{S}_z . The implementation of the QEE scheme requires $N_q = \lceil \log_2 Q \rceil < N$ qubits. Using the QEE isometry, configurations in \mathcal{F} are mapped to $\mathcal{Q} = \{|0\rangle_q, |1\rangle_q\}^{\otimes N_q}$, the computational basis states of a N_q -qubit system. To reduce the state preparation error,⁵³ a good practice in defining the QEE isometry \mathcal{E} is to first sort both \mathcal{F} and \mathcal{Q} in ascending order according to the electronic energy of $|\mathbf{f}\rangle_i$ and the decimal number associated to the binary string representing the qubit state. By doing so, a correspondence $\mathcal{E}|\mathbf{f}\rangle_i = |\mathbf{q}\rangle_i$ is established. We note that in general the size Q is not necessarily a power of 2. To fit the requirements of quantum circuits, unphysical states may therefore be included in QEE so as to build a Hilbert space with a size that is a power of 2. In this case, post-selection of

measurement results may be helpful to exclude results involving unphysical states.

In common Fermionic-to-qubit encoding schemes, there is a one to one correspondence of both creation and annihilation operators ($\hat{a}_p^\dagger, \hat{a}_q$) with qubit operators. In QEE, where by definition only states with fixed number of particles are considered, there is a one to one correspondence between the excitation operator $\hat{E}_{pq} \equiv \hat{a}_p^\dagger \hat{a}_q$ and a qubit operator \tilde{E}_{pq} , where the excitation operators are first rewritten as a sum of projection of Slater determinants $|\mathbf{f}_i\rangle \langle \mathbf{f}_j|$ and then transformed into qubit space through four entry operators: $\frac{1}{2}(X+iY), \frac{1}{2}(X-iY), \frac{1}{2}(I-Z), \frac{1}{2}(I+Z)$, see Ref⁵³ for detail. The qubit Hamiltonian can then be constructed using \tilde{E}_{pq} . For a generic Hamiltonian, where the projection operators would lead to a linear combination of up to an exponential number of Pauli operators, and in principle one needs to consider an exponentially large number of determinants, no quantum advantage would be achieved. QEE therefore should be considered as an intermediate solution for NISQ hardware. However, we note that both the size of the qubit Hamiltonian and the total number of Slater determinants scale polynomially as a function of N for the systems considered in our study, as we explain in the Section 3.1.

2.2 Qubit Coupled-Cluster Ansatz for Variational Quantum Eigensolvers

After constructing a qubit Hamiltonian using the QEE encoding, we discuss the choice of the wavefunction ansatz. One popular ansatz used in the literature is the unitary coupled-cluster (UCC) ansatz,^{8,68,69} inspired by coupled-cluster theory.⁷⁰ Such an ansatz can yield accurate results for many-body systems, but it leads to calculations suffering from poor scaling as a function of the number of gates, due to the inclusion of all possible electronic excitations. A typical implementation of the UCC ansatz on quantum computers leads to the following

expression in terms of Pauli strings (entanglers) \hat{P}_k :

$$\hat{U}_{\text{UCC}} = \prod_k \hat{U}_k = \prod_k e^{-i\theta_k \hat{P}_k/2}, \quad \hat{P}_k \in \{I, X, Y, Z\}^{\otimes N_q}. \quad (1)$$

The number of entanglers required when using the UCC ansatz may be large even for intermediate scale systems with $4 \sim 6$ electrons. The QCC ansatz⁵⁴ bypasses the formulation of the ansatz in physical space, and instead directly implements Eq. 1 in the qubit space. In particular, the QCC method proposed in Ref.⁵⁴ implements a screening process to select and retain the entanglers that contribute the most to the evaluation of the energy.

In QCC, the variation of the energy induced by each entangler is evaluated by expanding the energy to second order in the parameter θ_k :

$$\delta E[\theta_k; \hat{P}_k] = E[\theta_k; \hat{P}_k] - E_0 \approx \theta_k \left. \frac{dE[\theta_k; \hat{P}_k]}{d\theta_k} \right|_{\theta_k=0} + \frac{\theta_k^2}{2} \left. \frac{d^2 E[\theta_k; \hat{P}_k]}{d\theta_k^2} \right|_{\theta_k=0}, \quad (2)$$

where $E[\theta_k; \hat{P}_k] = \langle \Psi_0 | \hat{U}_k^\dagger \hat{H} \hat{U}_k | \Psi_0 \rangle$ and $E_0 = \langle \Psi_0 | \hat{H} | \Psi_0 \rangle$. The first derivative in Eq. 2 can be efficiently computed through quantum measurements as

$$\left. \frac{dE[\theta_k; \hat{P}_k]}{d\theta_k} \right|_{\theta_k=0} = \left\langle \Psi_0 \left| -\frac{i}{2} [\hat{H}, \hat{P}_k] \right| \Psi_0 \right\rangle, \quad (3)$$

which results from the similarity-transformed Hamiltonian being in closed form⁷¹

$$\hat{U}_k^\dagger \hat{H} \hat{U}_k = \hat{H} - i \frac{\sin \theta_k}{2} [\hat{H}, \hat{P}_k] + \frac{1}{2} (1 - \cos \theta_k) \hat{P}_k [\hat{H}, \hat{P}_k]. \quad (4)$$

The expression of the second order derivative can be found in Ref.⁵⁴

The implementation of the QCC method proceeds by ranking the entanglers according to the magnitude of their first-order derivative and sign of the second-order derivative, and by considering only the entanglers with highest rank. This amounts to screening the value of the first and second derivative of the energy for each of the $\sim 4^N$ entanglers and choosing those

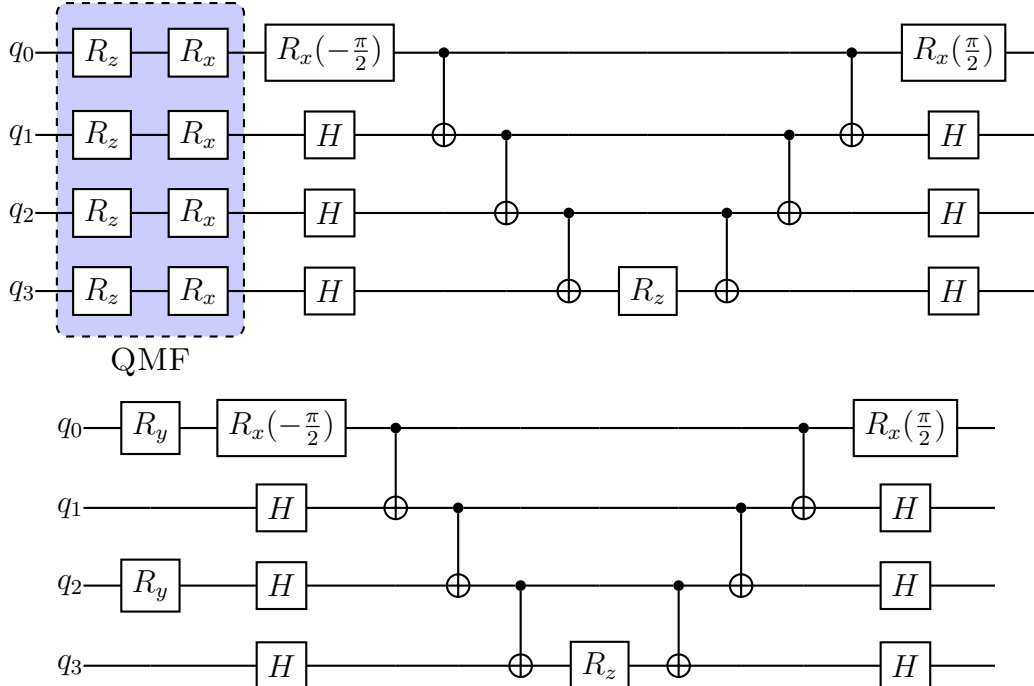


Figure 2: The upper panel shows a representative quantum circuit representing the qubit coupled-cluster ansatz with 4 qubits. The box circled by the dashed line shows the qubit mean-field (QMF) part of the circuit, which enables the construction of any product states. The circuit component following the QMF part enables the construction of the exponential of entangler $XXXY$, and it is built with the CNOT gate ladders. The lower panel shows a circuit representative of the modified ansatz, where the three entanglers are $IIYY, IYII, XXXY$, as defined in the pre-screening process.

with values of the first derivatives substantially different from zero or second derivatives substantially smaller than zero. By using a qubit basis state as $|\Psi_0\rangle$ we can reduce the dependency of the total number of \hat{P}_k with respect to the number of qubits from exponential to polynomial. The reduction is achieved by grouping the terms in the Hamiltonian and performing the pre-screening within each group; see Ref.⁷² for detail. In practice, the second derivatives could also be neglected to decrease computational cost,⁷² as we did in this work.

The quantum circuit is finally constructed using a ladder-like block procedure,⁷³ as shown in Fig. 2. As pointed out by Ref.,⁵⁴ for molecules like LiH and H₂O, the two-qubit gate count is greatly reduced compared to that of the UCC ansatz by bypassing any explicit Fermionic construction of electronic excitations and thus saving as many quantum resources as possible.

In the original proposal of the QCC⁵⁴ method, only entanglers with more than one non-

identity gate (X, Y, Z) were considered, and the quantum circuit was started with a qubit mean-field (QMF) component, as shown in Fig. 2. This QMF component consists of single R_x and R_z rotations on each qubit, allowing for access to any point on the Bloch sphere. Although it remains to be investigated whether such an implementation suffers from the Barren plateau problem,⁷⁴ the QMF component resembles the hardware-efficient ansatz²⁷ and might pose optimization challenges⁷⁵ due to the large number of required variational parameters ($2N_q$). In addition, R_x and R_z rotations are likely redundant degrees of freedom, since often times both the Hamiltonian and wavefunction of many-body systems of interest are real.

To solve the potential optimization challenges introduced by the QMF component, we propose a modification of the original QCC ansatz. We simply discard the QMF component, and consider all the possible entanglers when performing the screening operation, regardless of the number of qubits that the entangler involves. In this way, the number of necessary variational parameters are reduced and eventually a quantum circuit only contains exponentials of entanglers, as shown in the bottom panel of Fig. 2.

The QCC ansatz is suitable for NISQ devices, where a trade off between circuit depth and number of quantum measurements is desirable. We note that similar ideas to construct efficient ansatz circuits using gradient methods have been explored in recent years, including iterative QCC,⁷² ADAPT-VQE and its several variants,^{76,77} e.g. ClusterVQE,⁷⁸ factorized-form of UCC,⁷⁹ and projective quantum eigensolver.⁸⁰ Besides being hardware friendly, an additional benefit of the QCC ansatz is that it leads to differentiable potential energy surfaces given its functional dependence on the entanglers, and the gradients can be estimated using the parameter-shift rule.^{81,82} The QCC ansatz has shown the correct size-consistent behavior when applied to study the dissociation of H_2 , LiH and H_2O in Ref.⁵⁴ However, there is no guarantee that it will always yield the correct behavior for any systems since it depends on how the entanglers are truncated when the circuit is constructed. We also speculate that in general size-extensivity may be satisfied as entanglers for noninteracting fragments act only

on each fragment, and, therefore, commute and we thus have $E(2A) = 2E(A)$.

2.3 Quantum Subspace Expansion for Excitation Energies

We now turn to the discussion of the calculations of excitation energies, for which subspace type methods^{83–88} are suitable. These methods can be viewed as a quantum analog of CI and its variants, e.g., selected CI approach.⁸⁹ Here we choose the quantum subspace expansion (QSE) algorithm,^{83,84,90} which uses the same quantum circuit as the one to obtain the ground state and involves only additional quantum measurements.⁸⁴ Specifically for the ground state $|\Psi\rangle$, a set of expansion operators $\{\hat{O}_i\}$ is chosen, which act on $|\Psi\rangle$ to form a basis given by $\{\hat{O}_i|\Psi\rangle\}$, where $\hat{O} \in \{\hat{a}_a^\dagger\hat{a}_i, \hat{a}_a^\dagger\hat{a}_b^\dagger\hat{a}_j\hat{a}_i | i, j \in \mathcal{A}; a, b \in \mathcal{V}\}$. We use this basis to evaluate the Hamiltonian and overlap matrix elements:

$$H_{ij}^{\text{QSE}} = \langle \Psi | \hat{O}_i^\dagger \hat{H} \hat{O}_j | \Psi \rangle, \quad S_{ij}^{\text{QSE}} = \langle \Psi | \hat{O}_i^\dagger \hat{O}_j | \Psi \rangle. \quad (5)$$

Note that the expansion operators are not limited to double excitations, and we did not include additional excitations as double ones are sufficient to obtain the FCI spectrum of our systems. Using the matrices defined above, we then solve the generalized eigenvalue problem in the well conditioned subspace given by $H^{\text{QSE}}C = S^{\text{QSE}}C\varepsilon$, where C is the matrix of eigenvectors and ε the diagonal matrix of eigenvalues. As mentioned in section 2.1, the QEE encoding is used to transform the excitation operators $\hat{a}_i^\dagger\hat{a}_j$ into Pauli strings acting on N_q qubits, and the matrix elements are evaluated as weighted sums of the expectation values of these Pauli strings. The cost of QSE has two components: i) determining the matrix elements through measurements, and ii) solving the generalized eigenvalue problem. In the QEE-QCC scheme adopted in this work, the measurement cost is negligible since the majority of Pauli operators have been measured already when computing the ground state. Therefore the cost of the QSE calculations mainly comes from ii). We also note that the effectiveness of QSE is achieved with a careful choice of creation and annihilation operators,

which would be facilitated by using chemical intuition, e.g., by identifying the most dominant excitations.

3 Results

In this section we present results for the many-body ground and excited states of the NV^- center in diamond, VV^0 and V_{Si}^- in 4H-SiC. Using the methods described in Sec. 2, we performed calculations on the *ibmq-guadalupe* quantum computer using the IBM Qiskit package.⁹¹ We have applied measurement error mitigation^{92,93} to all the measurements.

3.1 Reference results on classical hardware

We use QDET to obtain the effective second quantized Hamiltonian, which is then used as input for our quantum computations.⁵⁷⁻⁵⁹ As a first step we define a periodic supercell with hundreds of atoms, representing a crystal with a defect center embedded in it, and we compute its electronic structure using Kohn-Sham (KS) density functional theory (DFT) with the PBE functional, the G_0W_0 approximation, and the Quantum Espresso^{94,95} and WEST⁹⁶ codes. A subset of KS orbitals localized around the defect is then chosen based on the localization criterion defined in Ref.⁵⁸ This subset constitutes the so-called active space A spanned by the second quantized effective Fermionic Hamiltonian $\hat{H}_{\text{elec}} = \sum_{ij}^A t_{ij}^{\text{eff}} \hat{a}_i^\dagger \hat{a}_j + \frac{1}{2} \sum_{ijkl}^A v_{ijkl}^{\text{eff}} \hat{a}_i^\dagger \hat{a}_j^\dagger \hat{a}_l \hat{a}_k$. The effective two-body matrix elements v_{ijkl}^{eff} are computed using the constrained random-phase approximation (cRPA) method. The effective one-body matrix elements t_{ij}^{eff} are computed from the G_0W_0 Hamiltonian removing a double counting term. Notably, in Ref.⁵⁸ we rigorously derived an expression of the double counting term within the G_0W_0 approximation.

We computed the electronic structure of NV^- , VV^0 and V_{Si}^- using a 215-, 198- and 127-atom supercell, respectively. We performed restricted closed-shell plane wave DFT calculations with the optimized structure from unrestricted open-shell calculations. We used the PBE⁹⁷ exchange-correlation functional, SG15 norm-conserving pseudopotentials,⁹⁸ and a 50 Ry kinetic energy cutoff for the plane wave basis set. The active space was defined considering all KS orbitals with highest localization factor $L_V(\psi_n^{\text{KS}}) = \int_V |\psi_n^{\text{KS}}(\mathbf{x})|^2 d\mathbf{x}$, where

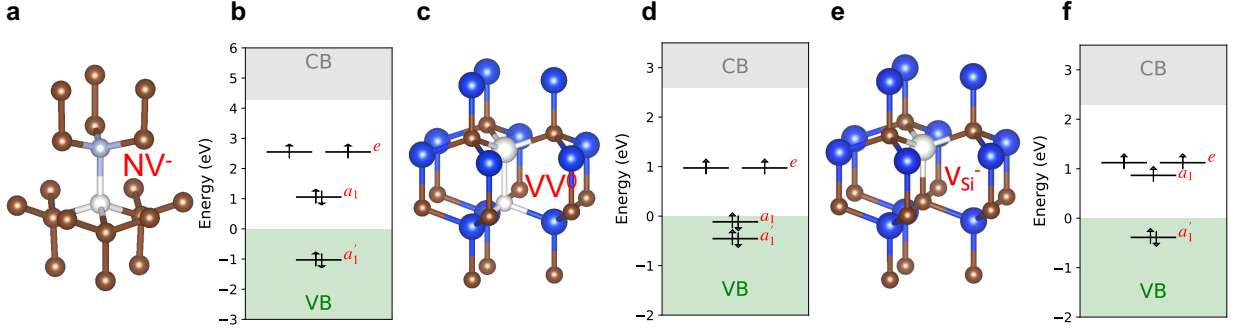


Figure 3: Spin defects studied in this work: the NV^- center in diamond, the VV^0 and V_{Si}^- in 4H-SiC. Panels **a**, **c** and **e** show a ball-and-stick representation of the defects. Panels **b**, **d** and **e** show single particle states obtained by solving the Kohn-Sham equations for the entire periodic solid, where gray and green shaded areas represent the conduction (CB) and valence band (VB), respectively; the single particles states are shown as black lines.

the integration is performed on a predefined volume V around the defect center (see Fig. 4), as originally defined in Ref. ⁵⁸ In our full-frequency G_0W_0 calculations we used 512 projective dielectric eigenpotentials (PDEPs) to represent the dielectric response. The QDET method is implemented in the WEST code. ^{96,99}

In Fig. 4 we show the convergence of vertical excitation energies of the three defects w.r.t. the localization threshold, which sets a lower bound for the KS orbitals to be included in the active spaces. We note that the energies are relatively well converged at 10%, 10% and 20% threshold in the three cases, corresponding to (14e, 8o), (22e, 12o) and (9e, 6o) active spaces, respectively. Due to the limitation in quantum resources, a compromise had to be made in selecting the active space to generate the effective Hamiltonians for the three defects: we chose the (14e, 8o) active space for VV^0 and NV^- . For NV^- , the convergence threshold for the (14e, 8o) active space lies between 20% and 10% and its excitation energies differ by approximately 0.1 eV from those obtained with a 10% localization threshold. Considering the complexity of the V_{Si}^- , for this defect we had to resort to a 30% localization threshold, leading to a (5e, 4o) active space, which we refer to as the “minimum model”.

We also note that when the localization threshold is lowered, the size of the active space N is increased by the inclusion of additional occupied orbitals. The total number of Slater

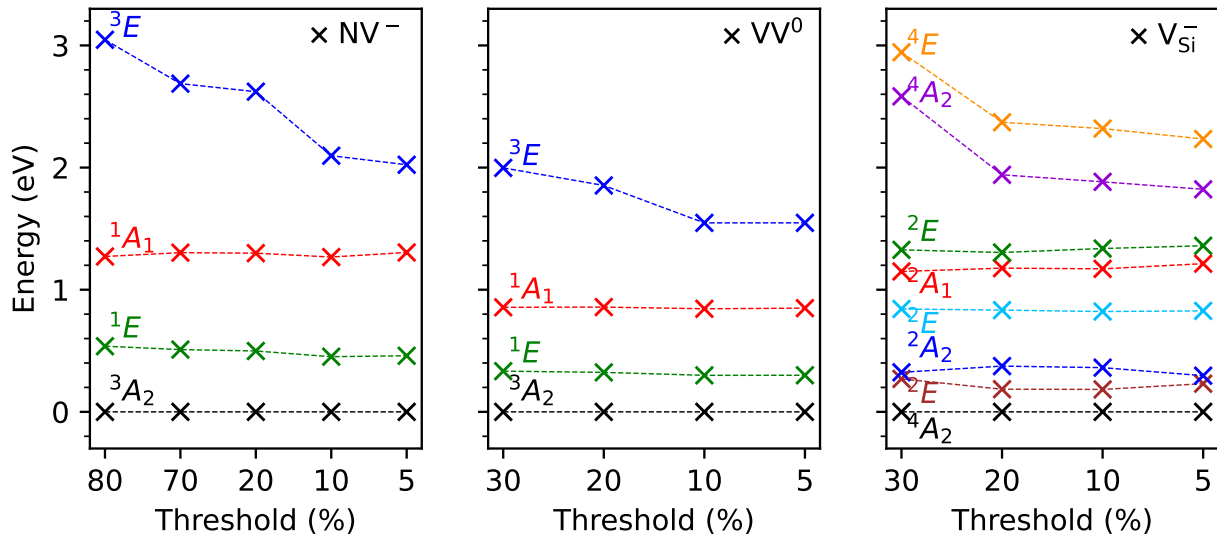


Figure 4: The left, middle and right panel show computed vertical excitation energies for the NV^- center in diamond, VV^0 and V_{Si}^- in 4H-SiC as a function of the chosen localization threshold. States are labeled using the irreducible representation of the C_{3v} point group. We note that the largest threshold corresponds to a (4e, 3o), (8e, 5o) or (5e, 4o) active space for the three defects, respectively, and the smallest threshold corresponds to a (26e, 14o), (64e, 33o) or (57e, 30o) active space, respectively.

determinants with a constant number of holes in each spin channel, $c_{\uparrow(\downarrow)} = \frac{N}{2} - m_{\uparrow(\downarrow)}$, scales polynomially as $O(N^{(c_{\uparrow}+c_{\downarrow})})$. This leads to an encoded effective Hamiltonian which is expressed as a linear combination of up to $O(N^{2(c_{\uparrow}+c_{\downarrow})})$ Pauli operators. The size of the QEE Hamiltonian and its corresponding classical preprocessing step do not pose a computational challenge for the systems considered here, where $c_{\uparrow(\downarrow)} \leq 2$.

3.2 Calculation of the ground state using a quantum computer

3.2.1 VV^0 in 4H-SiC and NV^- in diamond

The ground state of the effective Hamiltonian constructed for both the VV^0 in 4H-SiC and the NV^- center in diamond is a 3A_2 triplet state, whose $m_S = 0$ state has a multi-reference character. To obtain such a state on quantum computers using VQE, a good guess for the initial wavefunction is key to achieving fast convergence.⁴⁰ These systems are open-shell with the highest occupied molecular orbitals (HOMOs) in the active space being e orbitals; hence

it is wise to use $|\Psi_0\rangle = |..a_1\bar{a}_1e_x\bar{e}_y\rangle$ due to Hund’s Rule, where a_1, e_x, e_y (spin-up) and $\bar{a}_1, \bar{e}_x, \bar{e}_y$ (spin-down) denote the single particle orbitals in the active space, as shown in Fig. 3.

As mentioned above, we choose the (14e, 8o) active space for both defects, leading to a total of 64 Slater determinants, and requiring the use of 6 qubits to span the full qubit Hilbert space, i.e., $\mathcal{H}_{\text{eff}} \subseteq \mathcal{H}_q$. To construct the QCC ansatz, we first measure the energy gradients of different entanglers using Eq. 3. The amplitude of these gradients are obtained both on a real quantum device (noisy) and on a simulator (noiseless). They are listed in Tab. 1 for VV^0 . We find that the difference between noisy and noiseless results is negligible (within $1 \sim 2\%$). This is due to the fact that the measurement circuits does not contain two-qubit gates, which are major sources of error in NISQ devices. We also note that the four entanglers with top rank correspond to entanglers with the identity gate I at the two left-most qubit indices. Because of the chosen QEE scheme, the two left-most qubit indices control Slater determinants with the highest excitation energy, and originate from transitions from the lowest four occupied single particle orbitals. This suggests that we can use the frozen core approximation¹⁰⁰ to reduce the computational cost without sacrificing accuracy. Therefore we freeze the lowest four occupied orbital and in practice we work with 4 qubits, 4 entanglers, and a qubit Hamiltonian with 136 terms. The QCC circuit is constructed using 14 CNOT gates in total. The UCC counterpart, however, would require ~ 400 CNOT gates, indicating the critical advantage of the QCC method. For NV^- , the same logic applies and its circuit has 10 CNOT gates. Note that in the interest of generality, during the construction of the QCC ansatz, we did not take into consideration the point group symmetry of the ground state so as to design calculations that would be viable also for systems under strain or for moderately disordered lattices. If symmetry is invoked, both UCC and QCC can be reduced to a simple circuit with a single parameter and only two CNOT gates.⁴⁰

Results from the VQE optimization of VV^0 and NV^- are shown in the upper and middle panel of Fig. 5. The energy is evaluated on the quantum hardware as the weighted sum of the expectation values of Pauli strings, i.e., $E = \sum_i g_i \langle \hat{P}_i \rangle$. The expectation values of all

Table 1: Top entanglers for the electronic structure calculation of VV^0 and V_{Si}^- from Eqn. 3 before the frozen core approximation is carried out, with their magnitude computed using a noiseless simulator and a quantum hardware *ibmq_guadalupe* (Atomic units)

Rank	VV^0			V_{Si}^-		
	Entanglers	Noiseless	Noisy	Entanglers	Noiseless	Noisy
1	<i>IIIIXY</i>	0.009243	0.009170	<i>IXYII</i>	0.006969	0.006754
2	<i>IIXIYZ</i>	0.008177	0.008100	<i>IIIYI</i>	0.006693	0.006601
3	<i>IIXXIY</i>	0.008165	0.008065	<i>IIIIY</i>	0.004352	0.004352
4	<i>IIXIXY</i>	0.006587	0.006529	<i>IIIXY</i>	0.004350	0.004350

Pauli strings were obtained by measuring 8192 times N_c independent circuits so that the standard deviation (σ) of measurement is within 15 meV, where N_c is the number of groups that contain mutually commuting strings. In the case of VV^0 (NV^-), we find that the VQE calculation converges to a state that is ~ 0.5 (0.4) eV higher than the FCI reference energy obtained on a classical computer. The fluctuations are more pronounced for the NV^- center because our calculations were carried out at different times and the hardware environment was not identical for each measurement. The insets in Fig. 5, where the reference values are from noiseless simulations, show that in our optimization procedure we indeed converge to the ground state of the system. We find that for both VV^0 and NV^- , only the parameter associated with entangler *IIXY* is nonzero ($\pi/2$), indicating that the other ones are negligible in determining the ground state, thus reducing the circuit to one exponential block of *IIXY*. This simplified circuit is exactly what we obtained in Ref.⁴⁰ by taking into consideration the point group symmetry of the lattice.

To obtain an accurate estimate of the ground state energy, error mitigation is required and here we adopted the ZNE method. The latter is straightforward to implement and does not require additional qubits. The basic idea of ZNE is to amplify the noise of the circuit to various controllable levels and obtain the zero noise limit by extrapolation. The key to success of ZNE lies in how noise is artificially boosted. We employ a split exponential technique that we originally proposed in Ref.⁴⁰ to artificially increase the circuit depth of each exponential block $e^{i\theta_k \hat{P}_k}$ of the QCC quantum ansatz, i.e., n replicas are generated

with $\left(e^{i\frac{\theta_k}{n}\hat{P}_k}\right)^n$. We note that this technique is suitable for both UCC and QCC-type of ansatzes^{54,101-104} and it does not affect the Trotter error.⁴⁰ The extrapolation procedure is shown in Fig. 7. We worked with the reduced circuit with only one entangler $IIXY$, and considered $n = [1, 2, 3, 4, 5]$. For each value of n , we increased the measurements to 320000, so σ is kept within 2.5 meV and the stability of the extrapolation procedure is improved. A quadratic function is used for extrapolation and the difference between the ground state energy and the reference value obtained on a quantum simulator is one order of magnitude smaller than in the absence of ZNE.

3.2.2 V_{Si}^- in 4H-SiC

We now turn to the discussion of the V_{Si}^- spin defect in 4H-SiC, which has a $|^4A_2\rangle$ ground state, with multi-reference character for $m_s = \pm\frac{1}{2}$.⁵⁶ The HOMOs of V_{Si}^- consists of three quasi-degenerate orbitals: a_1, e_x, e_y that are all singly occupied in the ground state, as shown in Fig. 3. Therefore the $m_s = \pm\frac{1}{2}$ spin manifold is considerably more complicated than those of VV^0 and NV^- . We use only a minimal model of (5e, 4o) for the active space to describe this system, which is adequate to demonstrate the advantages of QCC over UCC in terms of finding the ground state with a shallow circuit depth. In this minimal model, the $m_s = \frac{1}{2}$ component of the ground state wavefunction consists of 6 Slater determinants

$$\begin{aligned} |\Psi_g\rangle = & \alpha (|a'_1\bar{a}'_1\bar{a}_1e_xe_y\rangle + |a'_1\bar{a}'_1a_1\bar{e}_xe_y\rangle + |a'_1\bar{a}'_1a_1e_x\bar{e}_y\rangle) \\ & + \beta (|\bar{a}'_1a_1\bar{a}_1e_xe_y\rangle + |a'_1a_1\bar{a}_1\bar{e}_xe_y\rangle + |a'_1a_1\bar{a}_1e_x\bar{e}_y\rangle), \end{aligned} \quad (6)$$

where we have only used two coefficients, α and β because of symmetry. From the FCI solutions on a classical computer we know that the first three configurations with doubly occupied a'_1 are dominant ($|\alpha| = 0.576$, $|\beta| = 0.0391$), hence we use one of them as the initial state of our VQE optimization. Specifically, we use $|\Psi_0\rangle = |a'_1\bar{a}'_1\bar{a}_1e_xe_y\rangle$.

When adopting the UCCSD ansatz, one needs to explicitly construct the relevant electronic excitations, whose associated parameters are $\theta_{a'_1}^{a_1}$, $\theta_{e_x\bar{a}_1}^{a_1\bar{e}_x}$, $\theta_{e_y\bar{a}_1}^{a_1\bar{e}_y}$, $\theta_{e_x\bar{a}'_1}^{a_1\bar{e}_x}$, $\theta_{e_y\bar{a}'_1}^{a_1\bar{e}_y}$. The result-

ing circuit requires ~ 200 CNOT gates, and with the UCCSD ansatz we only obtained the exact ground state on a noiseless simulator. A reasonable approximation is to assume $\beta = 0$, which would require only the first two parameters with a corresponding reduction of the number of CNOT gates to ~ 80 . This approximation leads to an error of ~ 11 meV, as shown in 6. However, both circuits are beyond the capability of NISQ quantum devices.

Here the QCC ansatz presents a remarkable advantage and we were able to simulate the V_{Si}^- defects on a real quantum processor. The screening of entanglers are summarized in Tab. 1. We selected the entanglers with top rank to construct the circuit for the ansatz, which contains only a total of 4 CNOT gates. The VQE optimization on a real quantum processor is shown in Fig. 5, where the error due to noise is about ~ 0.2 eV. We note that also in this case the ZNE is applied at the end of the VQE optimization to obtain a more accurate ground state energy, as shown in Fig. 7.

3.3 Calculation of the excited states using a quantum computer

As mentioned earlier, we computed excited states of the VV^0 and NV^- using the QSE algorithm. To avoid propagating the errors introduced by VQE, we used the exact energy of the 3A_2 state with $m_s = 0$ as the ground state energy.

We constructed a quantum subspace that is identical to the configuration state space, so the dimension of the QSE matrices is the same as that of their classical FCI counterpart. The QSE matrix is built by evaluating, on the quantum hardware, the expectation values of all Pauli strings. In our zero noise mitigation, we used a linear extrapolation for the off-diagonal elements of the QSE matrix and we computed diagonal elements with linear and quadratic extrapolations. The number of measurements was 320000 for both defects. The QSE matrix was finally diagonalized on a classical computer.

The errors of excitation energies with and without extrapolation are summarized in Fig. 8. The accuracy of the energy of non-degenerate excitations is in general improved when using the ZNE. We note that overall different choices of extrapolation functions lead to similar

results, and hence linear extrapolation is a desirable choice, since a smaller number of parameters is expected to lead to a more stable fit. The degeneracy of states is spuriously lifted on the quantum hardware due to the presence of noise, though it is slightly mitigated after applying the linear ZNE.

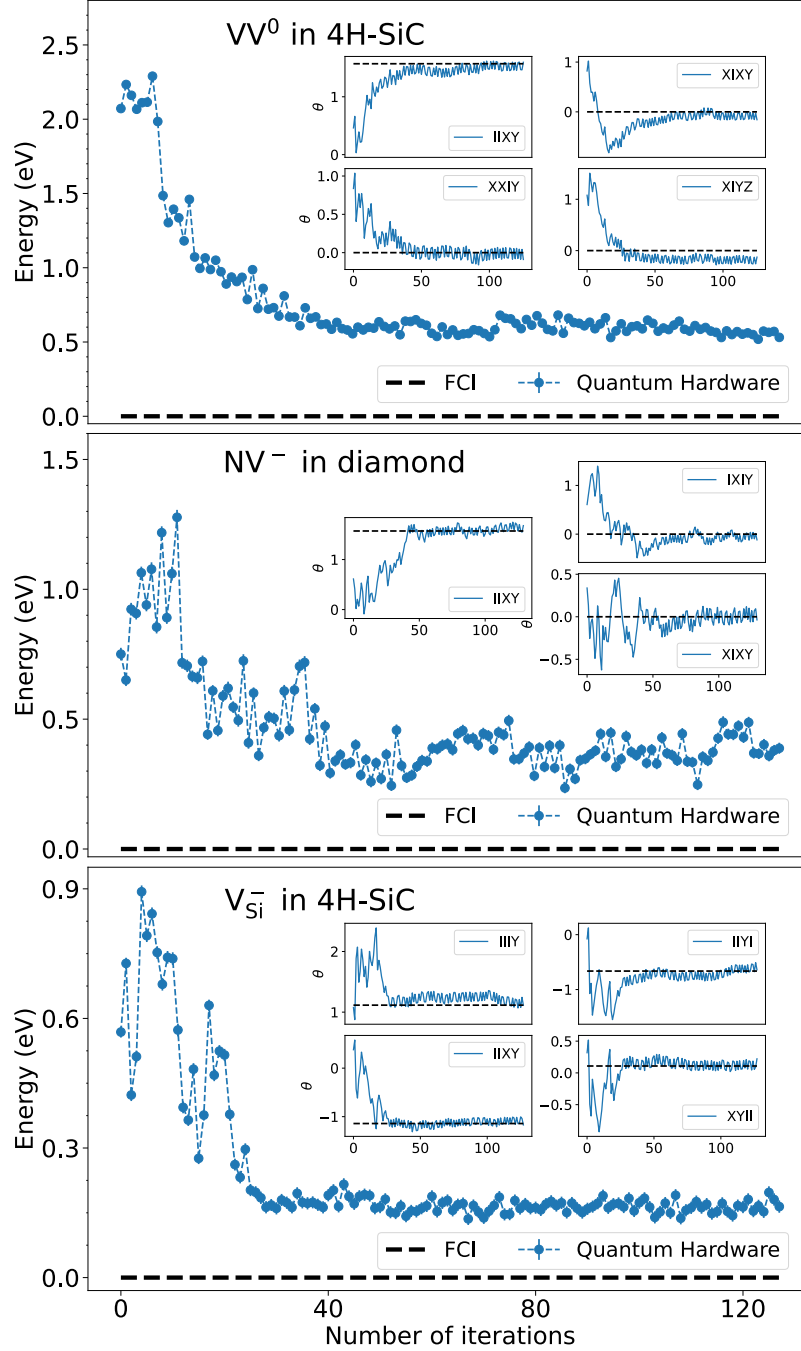


Figure 5: The upper, middle and bottom panel show the total energy as a function of the number of iterations during an optimization of the ground state energy of the VV^0 in 4H-SiC, the NV^- in diamond and the V_{Si}^- in 4H-SiC carried out with the variational quantum eigensolver (VQE) algorithm on *ibmq_guadalupe* (quantum hardware); the variation of parameters associated with each entangler of the qubit coupled cluster (QCC) ansatz is plotted in the inset. The full configuration interaction (FCI) energy is reported for reference.

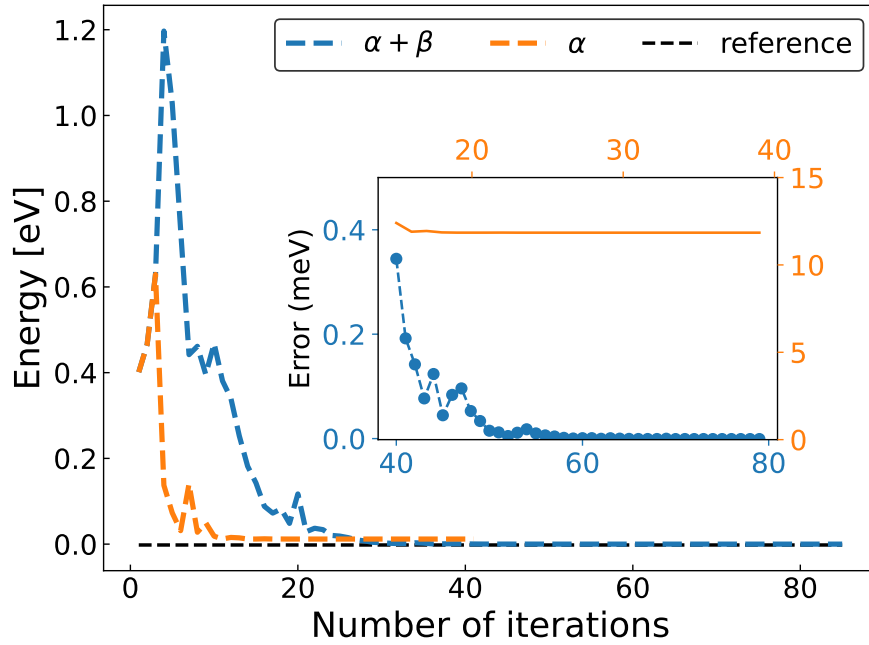


Figure 6: Total energy as a function of the number of iterations used to optimize the ground state energy of V_{Si}^- in 4H-SiC using the variational quantum eigensolver (VQE) algorithm on a noiseless simulator, with a unitary coupled cluster (UCC) ansatz and the COByLA optimizer.¹⁰⁵ The blue and orange curves represent results using two variants of the ansatz circuit with different levels of approximation; see text. The inset shows the error of different VQE optimizations relative to the reference energy. The full configuration interaction (FCI) energy (dashed black line) is reported for reference.

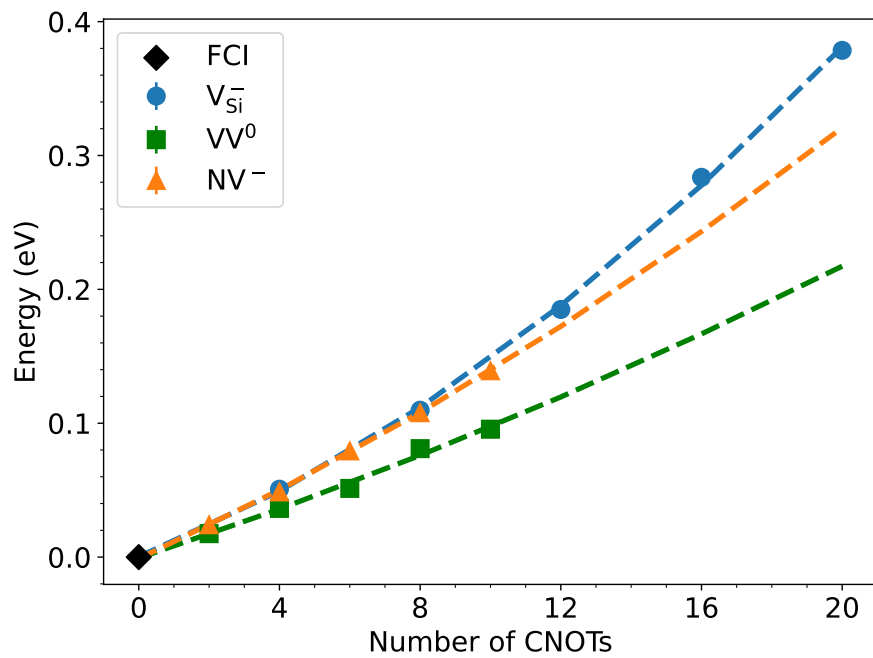


Figure 7: The ground state energy of the NV^- center and the VV^0 and V_{Si}^- in 4H-SiC as a function of the number of replicas used in the zero-noise extrapolation (see text), obtained using *ibmq_guadalupe*. The x axis is scaled with the number of CNOT gates used in the quantum circuit for clarity of comparison. The reference, noiseless result has been set to 0.

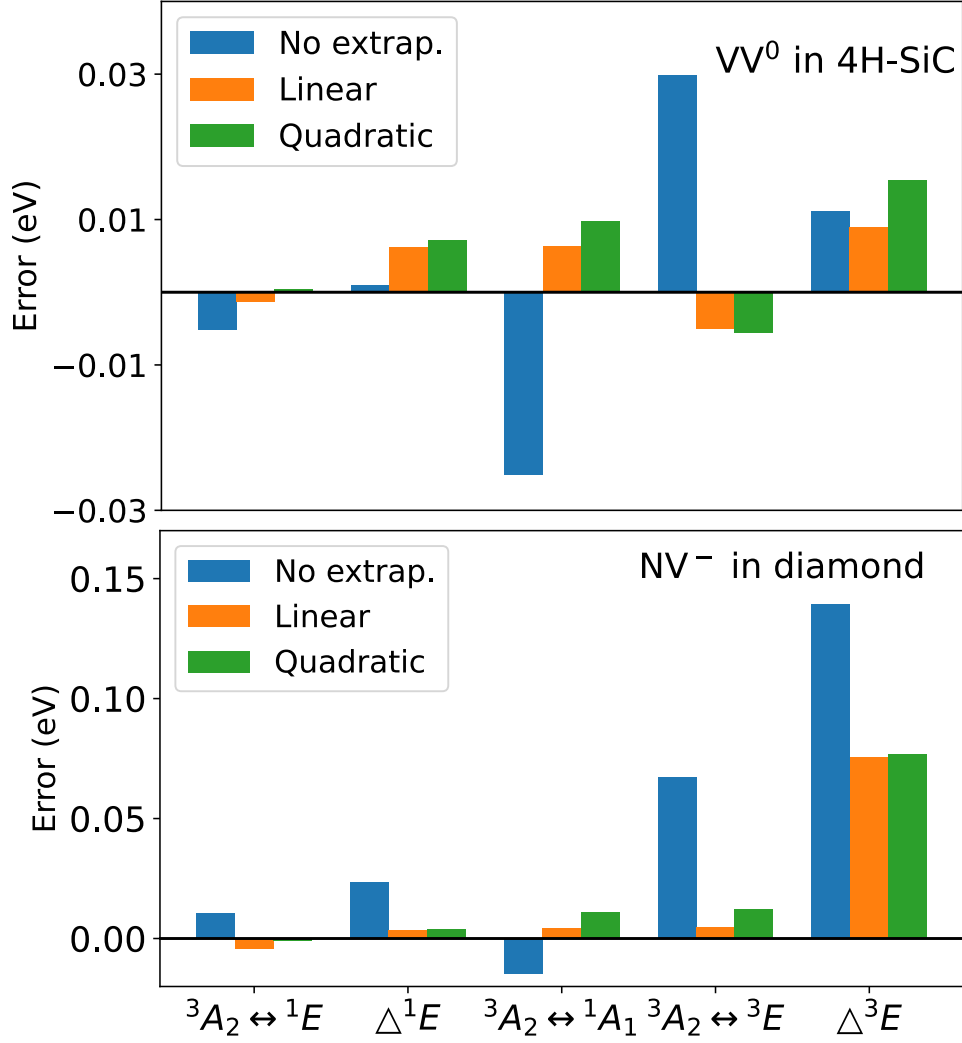


Figure 8: The upper and bottom panel show the error in the excitation energies (eV) of the VV^0 and NV^- defects calculated using the quantum subspace expansion (QSE) method on *ibmq-guadalupe*. The x axis shows transitions between states labeled using the representation of the point group C_{3v} , following Ref.³⁶ Δ^1E and Δ^3E indicate the breaking of degeneracy due to noise (see text). The reference values are obtained with a noiseless simulator and are identical to those of classical full configuration interaction (FCI) calculations on a classical computer. The blue, orange and green bar represent results obtained using no extrapolation, linear and quadratic zero-noise extrapolation techniques, respectively. For the results labeled with “quadratic extrapolation”, we only carried out a quadratic extrapolation for the diagonal elements of the QSE matrix elements, and a linear extrapolation was applied to the off-diagonal elements.

4 Conclusions

In summary, we presented a computational protocol to diagonalize Fermionic Hamiltonians on noisy-intermediate-quantum computers, which combines the QEE scheme to map electronic excitations onto qubits, a modified QCC ansatz for VQE optimizations of the ground state and noise mitigation techniques. The QEE mapping offers a robust solution to the unphysical state problem and the QCC ansatz provides a relatively short quantum circuit suitable for calculations on near-term intermediate-size quantum devices. We applied our protocol on quantum hardware to compute the electronic structure of strongly correlated ground and excited states of three spin defects, i.e., the NV^- center in diamond, the VV^0 and V_{Si}^- in 4H-SiC, and we presented calculations that would have been unfeasible with conventional algorithms. In particular, we could go beyond the minimum models for the NV^- and VV^0 and tackle a complex defects such as V_{Si}^- for the first time. Work is in progress to improve the efficiency of the measurements of $\langle H \rangle$ on quantum architectures, for example by adopting advanced measurements techniques with different term groupings,^{106,107} fragmentation procedures^{108,109} and classical shadow,^{110,111} and to extend the applicability of our protocol to larger active spaces appropriate, e.g. to investigate adsorbates on surfaces or ions and nanostructures in solution. We finally note that establishing which algorithms are better suited to achieve quantum advantage in electronic structure calculations remains an open area of research. For example, recent papers have argued that simulations in first quantization offer some important advantages over approaches in second quantization including faster convergence to the continuum limit and the opportunity for practical simulations beyond the Born-Oppenheimer approximation.¹¹² Interestingly, in addition to efforts towards reaching a practical advantage with quantum computers, the development of algorithms for quantum computations is having a positive impact on the development of classical algorithms in various fields, e.g., machine learning¹¹³ and computational spectroscopy.¹¹⁴

Acknowledgments

We thank Yu Jin for many fruitful discussions. We also thank the Qiskit Slack channel for generous help. This work was supported by the computational materials science center Midwest Integrated Center for Computational Materials (MICCoM) for the implementation and use of quantum embedding and by the Next Generation Quantum Science and Engineering (QNEXT) hub for the development of quantum algorithms and deployment on quantum hardware. MICCoM is part of the Computational Materials Sciences Program funded by the U.S. Department of Energy, Office of Science, Basic Energy Sciences, Materials Sciences, and Engineering Division through the Argonne National Laboratory, under Contract No. DE-AC02-06CH11357. QNEXT is supported by the U.S. Department of Energy, Office of Science, National Quantum Information Science Research Centers. This research used resources of the Oak Ridge Leadership Computing Facility at the Oak Ridge National Laboratory, which is supported by the Office of Science of the U.S. Department of Energy under Contract No. DE-AC05-00OR22725, resources of the National Energy Research Scientific Computing Center (NERSC), a DOE Office of Science User Facility supported by the Office of Science of the U.S. Department of Energy under Contract No. DE-AC02-05CH11231, and resources of the Argonne Leadership Computing Facility, which is a DOE Office of Science User Facility supported under Contract No. DE-AC02-06CH11357. We acknowledge the use of IBM Quantum services for this work and to advanced services provided by the IBM Quantum Researchers Program. The views expressed are those of the authors and do not reflect the official policy or position of IBM or the IBM Quantum team.

Author Contributions

B.H., M.G., and G.G. designed the research. N.S. performed the embedding calculations on classical computers. B.H. conducted the experiments on IBM quantum computers, with supervision by M.G. and G.G. All authors contributed to the writing of the manuscript.

Notes

The authors declare no competing interests.

References

- (1) Bell, A. T.; Head-Gordon, M. Quantum mechanical modeling of catalytic processes. *Annu. Rev. Chem. Biomol. Eng* **2011**, *2*, 453–477.
- (2) Xu, S.; Carter, E. A. Theoretical insights into heterogeneous (photo) electrochemical CO₂ reduction. *Chemical reviews* **2018**, *119*, 6631–6669.
- (3) Hammes-Schiffer, S.; Galli, G. Integration of theory and experiment in the modelling of heterogeneous electrocatalysis. *Nature Energy* **2021**, *6*, 700–705.
- (4) Jorgensen, W. L. The many roles of computation in drug discovery. *Science* **2004**, *303*, 1813–1818.
- (5) Ladd, T. D.; Jelezko, F.; Laflamme, R.; Nakamura, Y.; Monroe, C.; O’Brien, J. L. Quantum computers. *nature* **2010**, *464*, 45–53.
- (6) Degen, C. L.; Reinhard, F.; Cappellaro, P. Quantum sensing. *Reviews of Modern Physics* **2017**, *89*, 035002.
- (7) Aspuru-Guzik, A.; Dutoi, A. D.; Love, P. J.; Head-Gordon, M. Simulated quantum computation of molecular energies. *Science* **2005**, *309*, 1704–1707.
- (8) Peruzzo, A.; McClean, J.; Shadbolt, P.; Yung, M.-H.; Zhou, X.-Q.; Love, P. J.; Aspuru-Guzik, A.; O’Brien, J. L. A variational eigenvalue solver on a photonic quantum processor. *Nature communications* **2014**, *5*, 1–7.
- (9) Somma, R. D. Quantum eigenvalue estimation via time series analysis. *New Journal of Physics* **2019**, *21*, 123025.

- (10) Parrish, R. M.; McMahon, P. L. Quantum filter diagonalization: Quantum eigendecomposition without full quantum phase estimation. *arXiv preprint arXiv:1909.08925* **2019**,
- (11) Ge, Y.; Tura, J.; Cirac, J. I. Faster ground state preparation and high-precision ground energy estimation with fewer qubits. *Journal of Mathematical Physics* **2019**, *60*, 022202.
- (12) Motta, M.; Sun, C.; Tan, A. T.; O'Rourke, M. J.; Ye, E.; Minnich, A. J.; Brandão, F. G.; Chan, G. K. Determining eigenstates and thermal states on a quantum computer using quantum imaginary time evolution. *Nature Physics* **2020**, *16*, 205–210.
- (13) Lin, L.; Tong, Y. Heisenberg-limited ground-state energy estimation for early fault-tolerant quantum computers. *PRX Quantum* **2022**, *3*, 010318.
- (14) Huggins, W. J.; O'Gorman, B. A.; Rubin, N. C.; Reichman, D. R.; Babbush, R.; Lee, J. Unbiasing fermionic quantum Monte Carlo with a quantum computer. *Nature* **2022**, *603*, 416–420.
- (15) Cao, Y.; Romero, J.; Olson, J. P.; Degroote, M.; Johnson, P. D.; Kieferová, M.; Kivlichan, I. D.; Menke, T.; Peropadre, B.; Sawaya, N. P., et al. Quantum chemistry in the age of quantum computing. *Chemical reviews* **2019**, *119*, 10856–10915.
- (16) Kitaev, A. Y. Quantum measurements and the Abelian stabilizer problem. *arXiv preprint quant-ph/9511026* **1995**,
- (17) Abrams, D. S.; Lloyd, S. Simulation of many-body Fermi systems on a universal quantum computer. *Physical Review Letters* **1997**, *79*, 2586.
- (18) Abrams, D. S.; Lloyd, S. Quantum algorithm providing exponential speed increase for finding eigenvalues and eigenvectors. *Physical Review Letters* **1999**, *83*, 5162.

- (19) Lee, S.; Lee, J.; Zhai, H.; Tong, Y.; Dalzell, A. M.; Kumar, A.; Helms, P.; Gray, J.; Cui, Z.-H.; Liu, W., et al. Is there evidence for exponential quantum advantage in quantum chemistry? *arXiv preprint arXiv:2208.02199* **2022**,
- (20) Xu, X.; Li, Y. Quantum-assisted Monte Carlo algorithms for fermions. *arXiv preprint arXiv:2205.14903* **2022**,
- (21) Zhang, Y.; Huang, Y.; Sun, J.; Lv, D.; Yuan, X. Quantum Computing Quantum Monte Carlo. *arXiv preprint arXiv:2206.10431* **2022**,
- (22) Motta, M.; Zhang, S. Ab initio computations of molecular systems by the auxiliary-field quantum Monte Carlo method. *Wiley Interdisciplinary Reviews: Computational Molecular Science* **2018**, *8*, e1364.
- (23) Arute, F.; Arya, K.; Babbush, R.; Bacon, D.; Bardin, J. C.; Barends, R.; Biswas, R.; Boixo, S.; Brandao, F. G.; Buell, D. A., et al. Quantum supremacy using a programmable superconducting processor. *Nature* **2019**, *574*, 505–510.
- (24) Lanyon, B. P.; Whitfield, J. D.; Gillett, G. G.; Goggin, M. E.; Almeida, M. P.; Kasal, I.; Biamonte, J. D.; Mohseni, M.; Powell, B. J.; Barbieri, M., et al. Towards quantum chemistry on a quantum computer. *Nature chemistry* **2010**, *2*, 106–111.
- (25) O’Malley, P. J.; Babbush, R.; Kivlichan, I. D.; Romero, J.; McClean, J. R.; Barends, R.; Kelly, J.; Roushan, P.; Tranter, A.; Ding, N., et al. Scalable quantum simulation of molecular energies. *Physical Review X* **2016**, *6*, 031007.
- (26) Hempel, C.; Maier, C.; Romero, J.; McClean, J.; Monz, T.; Shen, H.; Jurcevic, P.; Lanyon, B. P.; Love, P.; Babbush, R., et al. Quantum chemistry calculations on a trapped-ion quantum simulator. *Physical Review X* **2018**, *8*, 031022.
- (27) Kandala, A.; Mezzacapo, A.; Temme, K.; Takita, M.; Brink, M.; Chow, J. M.; Gam-

- betta, J. M. Hardware-efficient variational quantum eigensolver for small molecules and quantum magnets. *Nature* **2017**, *549*, 242–246.
- (28) Kandala, A.; Temme, K.; Córcoles, A. D.; Mezzacapo, A.; Chow, J. M.; Gambetta, J. M. Error mitigation extends the computational reach of a noisy quantum processor. *Nature* **2019**, *567*, 491–495.
- (29) Smart, S. E.; Mazziotti, D. A. Quantum-classical hybrid algorithm using an error-mitigating N-representability condition to compute the Mott metal-insulator transition. *Physical Review A* **2019**, *100*, 022517.
- (30) Quantum, G. A.; Collaborators*†; Arute, F.; Arya, K.; Babbush, R.; Bacon, D.; Bardin, J. C.; Barends, R.; Boixo, S.; Broughton, M.; Buckley, B. B., et al. Hartree-Fock on a superconducting qubit quantum computer. *Science* **2020**, *369*, 1084–1089.
- (31) Yeter-Aydeniz, K.; Pooser, R. C.; Siopsis, G. Practical quantum computation of chemical and nuclear energy levels using quantum imaginary time evolution and Lanczos algorithms. *npj Quantum Information* **2020**, *6*, 1–8.
- (32) Smart, S. E.; Mazziotti, D. A. Quantum solver of contracted eigenvalue equations for scalable molecular simulations on quantum computing devices. *Physical Review Letters* **2021**, *126*, 070504.
- (33) Smart, S. E.; Boyn, J.-N.; Mazziotti, D. A. Resolving correlated states of benzyne with an error-mitigated contracted quantum eigensolver. *Physical Review A* **2022**, *105*, 022405.
- (34) Eddins, A.; Motta, M.; Gujarati, T. P.; Bravyi, S.; Mezzacapo, A.; Hadfield, C.; Sheldon, S. Doubling the size of quantum simulators by entanglement forging. *PRX Quantum* **2022**, *3*, 010309.

- (35) Huang, R.; Li, C.; Evangelista, F. A. Leveraging small scale quantum computers with unitarily downfolded Hamiltonians. *arXiv preprint arXiv:2208.08591* **2022**,
- (36) Ma, H.; Govoni, M.; Galli, G. Quantum simulations of materials on near-term quantum computers. *npj Computational Materials* **2020**, *6*, 1–8.
- (37) Cerasoli, F. T.; Sherbert, K.; Sławińska, J.; Nardelli, M. B. Quantum computation of silicon electronic band structure. *Physical Chemistry Chemical Physics* **2020**, *22*, 21816–21822.
- (38) Sherbert, K.; Cerasoli, F.; Nardelli, M. B. A systematic variational approach to band theory in a quantum computer. *RSC advances* **2021**, *11*, 39438–39449.
- (39) Yamamoto, K.; Manrique, D. Z.; Khan, I. T.; Sawada, H.; Ramo, D. M. Quantum hardware calculations of periodic systems with partition-measurement symmetry verification: Simplified models of hydrogen chain and iron crystals. *Physical Review Research* **2022**, *4*, 033110.
- (40) Huang, B.; Govoni, M.; Galli, G. Simulating the electronic structure of spin defects on quantum computers. *PRX Quantum* **2022**, *3*, 010339.
- (41) McClean, J. R.; Romero, J.; Babbush, R.; Aspuru-Guzik, A. The theory of variational hybrid quantum-classical algorithms. *New Journal of Physics* **2016**, *18*, 023023.
- (42) Weber, J.; Koehl, W.; Varley, J.; Janotti, A.; Buckley, B.; Van de Walle, C.; Awschalom, D. D. Quantum computing with defects. *Proceedings of the National Academy of Sciences* **2010**, *107*, 8513–8518.
- (43) Wolfowicz, G.; Heremans, F. J.; Anderson, C. P.; Kanai, S.; Seo, H.; Gali, A.; Galli, G.; Awschalom, D. D. Quantum guidelines for solid-state spin defects. *Nature Reviews Materials* **2021**, *6*, 906–925.

- (44) Hsieh, S.; Bhattacharyya, P.; Zu, C.; Mittiga, T.; Smart, T.; Machado, F.; Kobrin, B.; Höhn, T.; Rui, N.; Kamrani, M., et al. Imaging stress and magnetism at high pressures using a nanoscale quantum sensor. *Science* **2019**, *366*, 1349–1354.
- (45) Anderson, C. P.; Glen, E. O.; Zeledon, C.; Bourassa, A.; Jin, Y.; Zhu, Y.; Vorwerk, C.; Crook, A. L.; Abe, H.; Ul-Hassan, J., et al. Five-second coherence of a single spin with single-shot readout in silicon carbide. *Science advances* **2022**, *8*, eabm5912.
- (46) Shi, F.; Zhang, Q.; Wang, P.; Sun, H.; Wang, J.; Rong, X.; Chen, M.; Ju, C.; Reinhard, F.; Chen, H., et al. Single-protein spin resonance spectroscopy under ambient conditions. *Science* **2015**, *347*, 1135–1138.
- (47) Sawaya, N. P.; Smelyanskiy, M.; McClean, J. R.; Aspuru-Guzik, A. Error sensitivity to environmental noise in quantum circuits for chemical state preparation. *Journal of Chemical Theory and Computation* **2016**, *12*, 3097–3108.
- (48) Huggins, W. J.; McClean, J. R.; Rubin, N. C.; Jiang, Z.; Wiebe, N.; Whaley, K. B.; Babbush, R. Efficient and noise resilient measurements for quantum chemistry on near-term quantum computers. *npj Quantum Information* **2021**, *7*, 1–9.
- (49) Li, Y.; Benjamin, S. C. Efficient variational quantum simulator incorporating active error minimization. *Physical Review X* **2017**, *7*, 021050.
- (50) Temme, K.; Bravyi, S.; Gambetta, J. M. Error mitigation for short-depth quantum circuits. *Physical Review Letters* **2017**, *119*, 180509.
- (51) Endo, S.; Benjamin, S. C.; Li, Y. Practical quantum error mitigation for near-future applications. *Physical Review X* **2018**, *8*, 031027.
- (52) Endo, S.; Cai, Z.; Benjamin, S. C.; Yuan, X. Hybrid quantum-classical algorithms and quantum error mitigation. *Journal of the Physical Society of Japan* **2021**, *90*, 032001.

- (53) Shee, Y.; Tsai, P.-K.; Hong, C.-L.; Cheng, H.-C.; Goan, H.-S. Qubit-efficient encoding scheme for quantum simulations of electronic structure. *Physical Review Research* **2022**, *4*, 023154.
- (54) Ryabinkin, I. G.; Yen, T.-C.; Genin, S. N.; Izmaylov, A. F. Qubit coupled cluster method: a systematic approach to quantum chemistry on a quantum computer. *Journal of Chemical Theory and Computation* **2018**, *14*, 6317–6326.
- (55) Kraus, H.; Soltamov, V.; Fuchs, F.; Simin, D.; Sperlich, A.; Baranov, P.; Astakhov, G.; Dyakonov, V. Magnetic field and temperature sensing with atomic-scale spin defects in silicon carbide. *Scientific reports* **2014**, *4*, 1–8.
- (56) Soykal, Ö.; Dev, P.; Economou, S. E. Silicon vacancy center in 4 H-SiC: Electronic structure and spin-photon interfaces. *Physical Review B* **2016**, *93*, 081207.
- (57) Ma, H.; Sheng, N.; Govoni, M.; Galli, G. Quantum embedding theory for strongly correlated states in materials. *Journal of Chemical Theory and Computation* **2021**, *17*, 2116–2125.
- (58) Sheng, N.; Vorwerk, C.; Govoni, M.; Galli, G. Green’s Function Formulation of Quantum Defect Embedding Theory. *Journal of Chemical Theory and Computation* **2022**, *18*, 3512–3522.
- (59) Vorwerk, C.; Sheng, N.; Govoni, M.; Huang, B.; Galli, G. Quantum embedding theories to simulate condensed systems on quantum computers. *Nature Computational Science* **2022**, *2*, 424–432.
- (60) Bravyi, S.; Gambetta, J. M.; Mezzacapo, A.; Temme, K. Tapering off qubits to simulate fermionic Hamiltonians. *arXiv preprint arXiv:1701.08213* **2017**,
- (61) Jordan, P.; Neumann, J. v.; Wigner, E. P. *The Collected Works of Eugene Paul Wigner*; Springer, 1993; pp 298–333.

- (62) Seeley, J. T.; Richard, M. J.; Love, P. J. The Bravyi-Kitaev transformation for quantum computation of electronic structure. *The Journal of chemical physics* **2012**, *137*, 224109.
- (63) Elfving, V. E.; Millaruelo, M.; Gámez, J. A.; Gogolin, C. Simulating quantum chemistry in the seniority-zero space on qubit-based quantum computers. *Physical Review A* **2021**, *103*, 032605.
- (64) Setia, K.; Chen, R.; Rice, J. E.; Mezzacapo, A.; Pistoia, M.; Whitfield, J. D. Reducing qubit requirements for quantum simulations using molecular point group symmetries. *Journal of Chemical Theory and Computation* **2020**, *16*, 6091–6097.
- (65) Kirby, W. M.; Hadi, S.; Kreshchuk, M.; Love, P. J. Quantum simulation of second-quantized Hamiltonians in compact encoding. *Physical Review A* **2021**, *104*, 042607.
- (66) Kirby, W.; Fuller, B.; Hadfield, C.; Mezzacapo, A. Second-Quantized Fermionic Operators with Polylogarithmic Qubit and Gate Complexity. *PRX Quantum* **2022**, *3*, 020351.
- (67) Chamaki, D.; Metcalf, M.; de Jong, W. A. Compact Molecular Simulation on Quantum Computers via Combinatorial Mapping and Variational State Preparation. *arXiv preprint arXiv:2205.11742* **2022**,
- (68) Romero, J.; Babbush, R.; McClean, J. R.; Hempel, C.; Love, P. J.; Aspuru-Guzik, A. Strategies for quantum computing molecular energies using the unitary coupled cluster ansatz. *Quantum Science and Technology* **2018**, *4*, 014008.
- (69) Grimsley, H. R.; Claudino, D.; Economou, S. E.; Barnes, E.; Mayhall, N. J. Is the trotterized uccsd ansatz chemically well-defined? *Journal of Chemical Theory and Computation* **2019**, *16*, 1–6.

- (70) Helgaker, T.; Jorgensen, P.; Olsen, J. *Molecular electronic-structure theory*; John Wiley & Sons, 2014.
- (71) Lang, R. A.; Ryabinkin, I. G.; Izmaylov, A. F. Unitary transformation of the electronic hamiltonian with an exact quadratic truncation of the baker-campbell-hausdorff expansion. *Journal of Chemical Theory and Computation* **2020**, *17*, 66–78.
- (72) Ryabinkin, I. G.; Lang, R. A.; Genin, S. N.; Izmaylov, A. F. Iterative qubit coupled cluster approach with efficient screening of generators. *Journal of Chemical Theory and Computation* **2020**, *16*, 1055–1063.
- (73) Barkoutsos, P. K.; Gonthier, J. F.; Sokolov, I.; Moll, N.; Salis, G.; Fuhrer, A.; Ganzhorn, M.; Egger, D. J.; Troyer, M.; Mezzacapo, A., et al. Quantum algorithms for electronic structure calculations: Particle-hole Hamiltonian and optimized wavefunction expansions. *Physical Review A* **2018**, *98*, 022322.
- (74) McClean, J. R.; Boixo, S.; Smelyanskiy, V. N.; Babbush, R.; Neven, H. Barren plateaus in quantum neural network training landscapes. *Nature communications* **2018**, *9*, 1–6.
- (75) Wang, S.; Fontana, E.; Cerezo, M.; Sharma, K.; Sone, A.; Cincio, L.; Coles, P. J. Noise-induced barren plateaus in variational quantum algorithms. *Nature communications* **2021**, *12*, 1–11.
- (76) Grimsley, H. R.; Economou, S. E.; Barnes, E.; Mayhall, N. J. An adaptive variational algorithm for exact molecular simulations on a quantum computer. *Nature communications* **2019**, *10*, 1–9.
- (77) Tang, H. L.; Shkolnikov, V.; Barron, G. S.; Grimsley, H. R.; Mayhall, N. J.; Barnes, E.; Economou, S. E. qubit-adapt-vqe: An adaptive algorithm for constructing hardware-efficient ansätze on a quantum processor. *PRX Quantum* **2021**, *2*, 020310.

- (78) Zhang, Y.; Cincio, L.; Negre, C. F.; Czarnik, P.; Coles, P.; Anisimov, P. M.; Mniszewski, S. M.; Tretiak, S.; Dub, P. A. Variational quantum eigensolver with reduced circuit complexity. *arXiv preprint arXiv:2106.07619* **2021**,
- (79) Chen, J.; Cheng, H.-P.; Freericks, J. K. Quantum-inspired algorithm for the factorized form of unitary coupled cluster theory. *Journal of Chemical Theory and Computation* **2021**, *17*, 841–847.
- (80) Stair, N. H.; Evangelista, F. A. Simulating many-body systems with a projective quantum eigensolver. *PRX Quantum* **2021**, *2*, 030301.
- (81) Crooks, G. E. Gradients of parameterized quantum gates using the parameter-shift rule and gate decomposition. *arXiv preprint arXiv:1905.13311* **2019**,
- (82) Schuld, M.; Bergholm, V.; Gogolin, C.; Izaac, J.; Killoran, N. Evaluating analytic gradients on quantum hardware. *Physical Review A* **2019**, *99*, 032331.
- (83) McClean, J. R.; Kimchi-Schwartz, M. E.; Carter, J.; De Jong, W. A. Hybrid quantum-classical hierarchy for mitigation of decoherence and determination of excited states. *Physical Review A* **2017**, *95*, 042308.
- (84) Colless, J. I.; Ramasesh, V. V.; Dahlen, D.; Blok, M. S.; Kimchi-Schwartz, M. E.; McClean, J. R.; Carter, J.; de Jong, W. A.; Siddiqi, I. Computation of molecular spectra on a quantum processor with an error-resilient algorithm. *Physical Review X* **2018**, *8*, 011021.
- (85) Epperly, E. N.; Lin, L.; Nakatsukasa, Y. A theory of quantum subspace diagonalization. *arXiv preprint arXiv:2110.07492* **2021**,
- (86) Tkachenko, N. V.; Zhang, Y.; Cincio, L.; Boldyrev, A. I.; Tretiak, S.; Dub, P. A. Quantum Davidson Algorithm for Excited States. *arXiv preprint arXiv:2204.10741* **2022**,

- (87) Cortes, C. L.; Gray, S. K. Quantum Krylov subspace algorithms for ground-and excited-state energy estimation. *Physical Review A* **2022**, *105*, 022417.
- (88) Kirby, W.; Motta, M.; Mezzacapo, A. Exact and efficient Lanczos method on a quantum computer. *arXiv preprint arXiv:2208.00567* **2022**,
- (89) Buenker, R. J.; Peyerimhoff, S. D. Individualized configuration selection in CI calculations with subsequent energy extrapolation. *Theoretica chimica acta* **1974**, *35*, 33–58.
- (90) McArdle, S.; Endo, S.; Aspuru-Guzik, A.; Benjamin, S. C.; Yuan, X. Quantum computational chemistry. *Reviews of Modern Physics* **2020**, *92*, 015003.
- (91) Aleksandrowicz, G., et al. Qiskit: An open-source framework for quantum computing. **2019**,
- (92) Dewes, A.; Ong, F. R.; Schmitt, V.; Lauro, R.; Boulant, N.; Bertet, P.; Vion, D.; Esteve, D. Characterization of a two-transmon processor with individual single-shot qubit readout. *Physical Review Letters* **2012**, *108*, 057002.
- (93) Maciejewski, F. B.; Zimborás, Z.; Oszmaniec, M. Mitigation of readout noise in near-term quantum devices by classical post-processing based on detector tomography. *Quantum* **2020**, *4*, 257.
- (94) Giannozzi, P.; Baroni, S.; Bonini, N.; Calandra, M.; Car, R.; Cavazzoni, C.; Ceresoli, D.; Chiarotti, G. L.; Cococcioni, M.; Dabo, I., et al. QUANTUM ESPRESSO: a modular and open-source software project for quantum simulations of materials. *Journal of physics: Condensed matter* **2009**, *21*, 395502.
- (95) Giannozzi, P.; Andreussi, O.; Brumme, T.; Bunau, O.; Nardelli, M. B.; Calandra, M.; Car, R.; Cavazzoni, C.; Ceresoli, D.; Cococcioni, M., et al. Advanced capabilities

- for materials modelling with Quantum ESPRESSO. *Journal of physics: Condensed matter* **2017**, *29*, 465901.
- (96) Govoni, M.; Galli, G. Large scale GW calculations. *Journal of Chemical Theory and Computation* **2015**, *11*, 2680–2696.
- (97) Perdew, J. P.; Burke, K.; Ernzerhof, M. Generalized gradient approximation made simple. *Physical Review Letters* **1996**, *77*, 3865.
- (98) Schlipf, M.; Gygi, F. Optimization algorithm for the generation of ONCV pseudopotentials. *Computer Physics Communications* **2015**, *196*, 36–44.
- (99) Yu, V. W.-z.; Govoni, M. GPU Acceleration of Large-Scale Full-Frequency GW Calculations. *Journal of Chemical Theory and Computation* **2022**, *18*, 4690–4707, PMID: 35913080.
- (100) Rossmannek, M.; Barkoutsos, P. K.; Ollitrault, P. J.; Tavernelli, I. Quantum HF/DFT-embedding algorithms for electronic structure calculations: Scaling up to complex molecular systems. *The Journal of Chemical Physics* **2021**, *154*, 114105.
- (101) Lee, J.; Huggins, W. J.; Head-Gordon, M.; Whaley, K. B. Generalized unitary coupled cluster wave functions for quantum computation. *Journal of Chemical Theory and Computation* **2018**, *15*, 311–324.
- (102) Metcalf, M.; Bauman, N. P.; Kowalski, K.; De Jong, W. A. Resource-efficient chemistry on quantum computers with the variational quantum eigensolver and the double unitary coupled-cluster approach. *Journal of Chemical Theory and Computation* **2020**, *16*, 6165–6175.
- (103) Liu, J.; Cheng, L. Unitary coupled-cluster based self-consistent polarization propagator theory: A quadratic unitary coupled-cluster singles and doubles scheme. *The Journal of Chemical Physics* **2021**, *155*, 174102.

- (104) Fedorov, D. A.; Alexeev, Y.; Gray, S. K.; Otten, M. Unitary Selective Coupled-Cluster Method. *Quantum* **2022**, *6*, 703.
- (105) Powell, M. J. *Advances in optimization and numerical analysis*; Springer, 1994; pp 51–67.
- (106) Gui, K.; Tomesh, T.; Gokhale, P.; Shi, Y.; Chong, F. T.; Martonosi, M.; Suchara, M. Term grouping and travelling salesperson for digital quantum simulation. *arXiv preprint arXiv:2001.05983* **2020**,
- (107) Yen, T.-C.; Ganeshram, A.; Izmaylov, A. F. Deterministic improvements of quantum measurements with grouping of compatible operators, non-local transformations, and covariance estimates. *arXiv preprint arXiv:2201.01471* **2022**,
- (108) Choi, S.; Yen, T.-C.; Izmaylov, A. F. Improving quantum measurements by introducing” ghost” Pauli products. *arXiv preprint arXiv:2208.06563* **2022**,
- (109) Choi, S.; Loaiza, I.; Izmaylov, A. F. Fluid fermionic fragments for optimizing quantum measurements of electronic Hamiltonians in the variational quantum eigensolver. *arXiv preprint arXiv:2208.14490* **2022**,
- (110) Huang, H.-Y.; Kueng, R.; Preskill, J. Predicting many properties of a quantum system from very few measurements. *Nature Physics* **2020**, *16*, 1050–1057.
- (111) Nakaji, K.; Endo, S.; Matsuzaki, Y.; Hakoshima, H. Measurement optimization of variational quantum simulation by classical shadow and derandomization. *arXiv preprint arXiv:2208.13934* **2022**,
- (112) Su, Y.; Berry, D. W.; Wiebe, N.; Rubin, N.; Babbush, R. Fault-tolerant quantum simulations of chemistry in first quantization. *PRX Quantum* **2021**, *2*, 040332.

- (113) Tang, E. A quantum-inspired classical algorithm for recommendation systems. Proceedings of the 51st Annual ACM SIGACT Symposium on Theory of Computing. 2019; pp 217–228.
- (114) Oh, C.; Lim, Y.; Wong, Y.; Fefferman, B.; Jiang, L. Quantum-inspired classical algorithm for molecular vibronic spectra. *arXiv preprint arXiv:2202.01861* **2022**,